IACMI/R000-2020/7.9

Thermal Instability in the Manufacturing of Wind Turbine Blade Spar Caps – Phase 2

Author: Rebecca Cutting
Anthony Favaloro
Johnathan Goodsell
Date: January 5, 2022

Final Technical Report
PA16-0349-7.9-01

Approved for Public Release.
Distribution is Unlimited.

The Institute for iacmi Advanced Composites Manufacturing Innovation
THE COMPOSITES INSTITUTE
U.S. DEPARTMENT OF ENERGY

The information, data, or work presented herein was funded in part by the Office of Energy Efficiency and Renewable Energy (EERE), U.S. Department of Energy, under Award DE-EE0006926

Thermal Instability in the Manufacturing of Wind Turbine Blade Spar Caps – Phase 2

Principal Investigator: Rebecca Cutting

Organization: Purdue University – Composites Manufacturing and Simulation Center

Address: 1105 Challenger Ave, Suite 100, West Lafayette, IN 47906

Phone:

Email: rcutting@purdue.edu

Co-authors:

- Anthony Favaloro, Purdue University College of Engineering, Composites Manufacturing and Simulation Center, West Lafayette, Indiana, 47906
- Johnathan Goodsell, Purdue University College of Engineering, Composites Manufacturing and Simulation Center, West Lafayette, Indiana, 47906

Date Published: (January, 2022)

Prepared by:
Institute for Advanced Composites Manufacturing Innovation
Knoxville, TN 37932
Managed by Collaborative Composite Solutions, Inc.
For the
U.S. DEPARTMENT OF ENERGY
Under contract DE- EE0006926

Project Period:
(06/2020 – 7/2021)

Approved For Public Release

TABLE OF CONTENTS

1. LISTS

1.1 List of Acronyms

CMSC – Composites Manufacturing and Simulation Center
DOC – Degree of cure
DSC – Differential scanning calorimetry
FEM – Finite element model
VARTM – Vacuum assisted resin transfer molding
erfh5 – PAM-RTM results file extension

1.2 List of Figures

1.3 List of Tables

2. EXECUTIVE SUMMARY

As the wind turbine industry continues to develop, the technology surrounding the design, development, and manufacturing of blades requires advancement as well. Wind turbine blades continue to increase in size, increasing the cost and time associated with manufacturing. Simulation driven manufacturing cycle design is required for the industry to maintain manufacturing schedules and optimize the manufacturing process.

A recent effort to reduce the cycle time of wind blade spar caps encountered a recurring manufacturing defect during the exotherm and curing of the resin system after filling in the vacuum-assisted resin transfer molding (VARTM) process. Thermal waves developed in sections of the spar cap resulting in unacceptable part tolerances, requiring the parts to be thrown out. The first phase of this IACMI project focused on characterizing the fabric and epoxy system used in manufacturing and simulating the manufacturing process to determine the root cause of the thermal waves. The second phase of this project refined and validated the manufacturing simulations. The simulation workflow was then used to analyze multiple cure cycle options to determine if the thermal waves would appear.

The estimated filling time from the filling simulation was shown to match well to experiment, and the temperature history from the curing simulation lined up well with experiment. This indicates that these simulations could be used to evaluate future curing cycles to be used with manufacturing. It is recommended that the distortion simulation work be completed for this project, as it would allow for further manufacturing cycle evaluation through the prediction of stresses and strains in the part. This could provide indicators of defects like the thermal waves seen in manufacturing earlier.

3. INTRODUCTION

This report provides details about the testing and simulation completed for Phase 2 of the IACMI 7.9 project between TPI Composites and Purdue University with the goal of using simulation to predict the buckling behavior seen in wind turbine spar cap manufacturing [1]. The goal of Phase 2 work was to create a multi-physics simulation that could capture infusion, heat transfer, cure kinetics, rheological advancement, and thermo-mechanics of the composite spar cap during manufacturing. A well-developed simulation workflow could be used to optimize the resin transfer molding manufacturing process.

This report will first review the material characterization of the resin system via differential scanning calorimetry (DSC) and rheometry tests. The fiberglass permeability and cured mechanical properties were characterized in the first phase of this project [1]. The filling simulation setup in ESI's PAM-FORM [2] will be described next, followed by the curing simulation in Abaqus. Future work, including the distortion simulation will also be discussed. Large parts of this report are taken from the conference paper "Multi-Physics Manufacturing Simulation of 60-Meter Wind Turbine Spar Cap" that was presented at CAMX 2021 [3].

4. MATERIAL CHARACTERIZATION

Material characterization was necessary to predict the filling time and cure distribution of the spar

cap. The resin system used in this work was Hexion EPIKOTE MGS RIMR 035c with an Epikure Curing Agent RIMH038. The resin to hardener mixture was 100:28 by weight. An Owens Corning 1800 GSM unidirectional stitched glass fabric was used as the fiber form.

4.1 Previous Material Characterization

Phase 1 of this project reported [1] on material characterization of resin properties like the cure kinetics, viscosity, storage modulus, and cure shrinkage. The cure kinetics and viscosity experiments were repeated in this phase of the work because Phase 1 tested the resin systems at temperatures greater than 60°C while the temperatures during filling averaged around 30°C. The additional testing was necessary to characterize the resin behavior at manufacturing temperatures.

The previous phase of this project also characterized the fiberglass permeability and the composite mechanical and thermal properties like fiber volume fraction, orthotropic Young's modulus values, and coefficients of thermal expansion. Unless stated otherwise, the properties used in the simulations for this work were provided by the previous characterization testing of this project.

4.2 Cure Kinetics

Cure kinetics characterization was performed with a DSC at the Composites Manufacturing and Simulation Center (CMSC) at Purdue University. A sample of mixed epoxy, between 12 to 20 mg, was placed inside a sealed aluminum pan and kept at constant temperature to monitor the heat flow of the sample over time. Isothermal runs were completed at 35 °C, 45 °C, 55 °C, and 65 °C. The heat flow time histories obtained from the DSC were each normalized by the sample's mass, then integrated with respect to time. A post-cure ramp in temperature revealed no additional heat flow, so the samples were assumed to be fully cured. Therefore, the integrated heat flow curves were normalized to be fully cured at the end of the isothermal run. This gave an estimate for the degree of cure (DOC) versus time.

The DOC curves were then fit to a simplified autocatalytic model represented with an Arrhenius function defined by [4]

$$\dot{\alpha} = A \exp\left(-\frac{E}{RT}\right)(1-\alpha)^n \tag{1}$$

Where α is the degree of cure, A is the frequency factor, R is the ideal gas constant, T is temperature, and E is activation energy. Figure 1 shows the cure development for the experimental DSC samples versus the autocatalytic model. The autocatalytic model cures a bit faster than experiment for the 35 °C, 55 °C, and 65 °C cases, but the model follows overall trends for each of the isothermal runs. The parameters fit to the autocatalytic model are provided in Table 1.

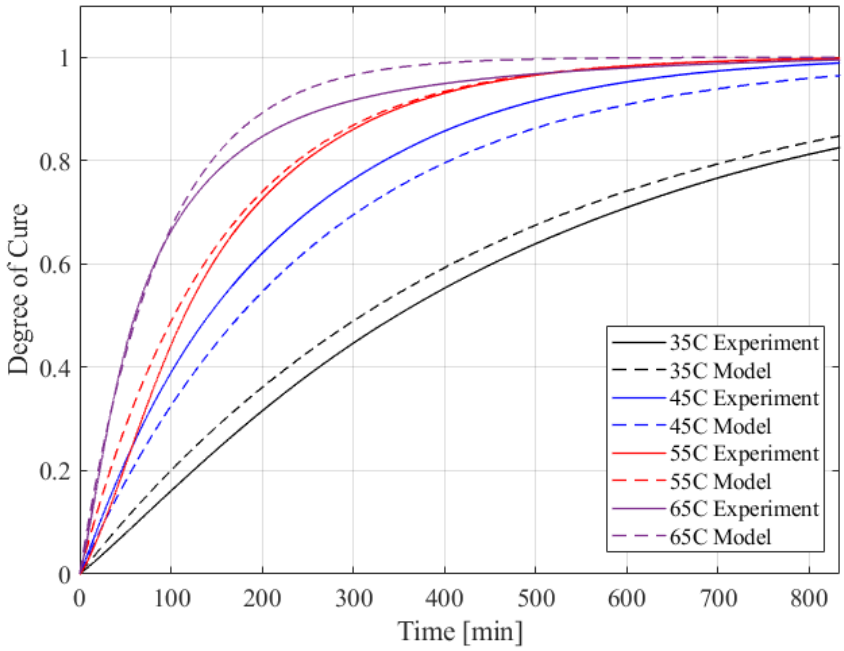

Figure 1: Comparison of experimental and autocatalytic model cure development for Hexion EPIKOTE MGS RIMR 035c with an Epikure Curing Agent RIMH038

Table 1: Autocatalytic model parameters that were fit to the isothermal DSC runs

Parameter	Value
A $[s^{-1}]$	2.37e3
E/R $[K]$	5537
N	0.9878

4.3 Viscosity

The viscosity of the resin is dependent upon the degree of cure, which changes during the filling process. Therefore, the viscosity needed to be characterized across a range of temperatures seen during manufacturing. A series of tests were performed with a parallel plate rheometer to determine the viscosity of the neat resin as a function of degree of cure and temperature. The tests were completed in a strain control mode with 1% strain at 20 rad/sec. Three isothermal runs, at 35 °C, 45 °C, and 90 °C, captured how the viscosity of the resin changed with time. The 90°C run was completed in the previous phase of the project. The raw viscosity data combined with the cure kinetics model allowed for the fitting of the Castro-Macosko model [5] which is represented with

$$\mu(T,\alpha) = \mu(\mathrm{T})\frac{\alpha_g}{\alpha_g - \alpha}^{C_1 + C_2\alpha} \quad (2)$$

$$\text{Where } \mu(T) = C_\tau \exp\left(\frac{T_g}{T}\right) \quad (3)$$

In these equations, μ is the viscosity, T is the temperature, α is the degree of cure, T_g is the glass

transition temperature, α_g is the degree of cure at glass transition, and the other variables are fitting parameters.

Figure 2 compares the raw data from the rheometer tests to the curves produced by the fit Castro-Macosko model. As can be seen, the model fits the data well for all temperatures tested. The fitted parameters for the Castro-Macosko model are provided in Table 2.

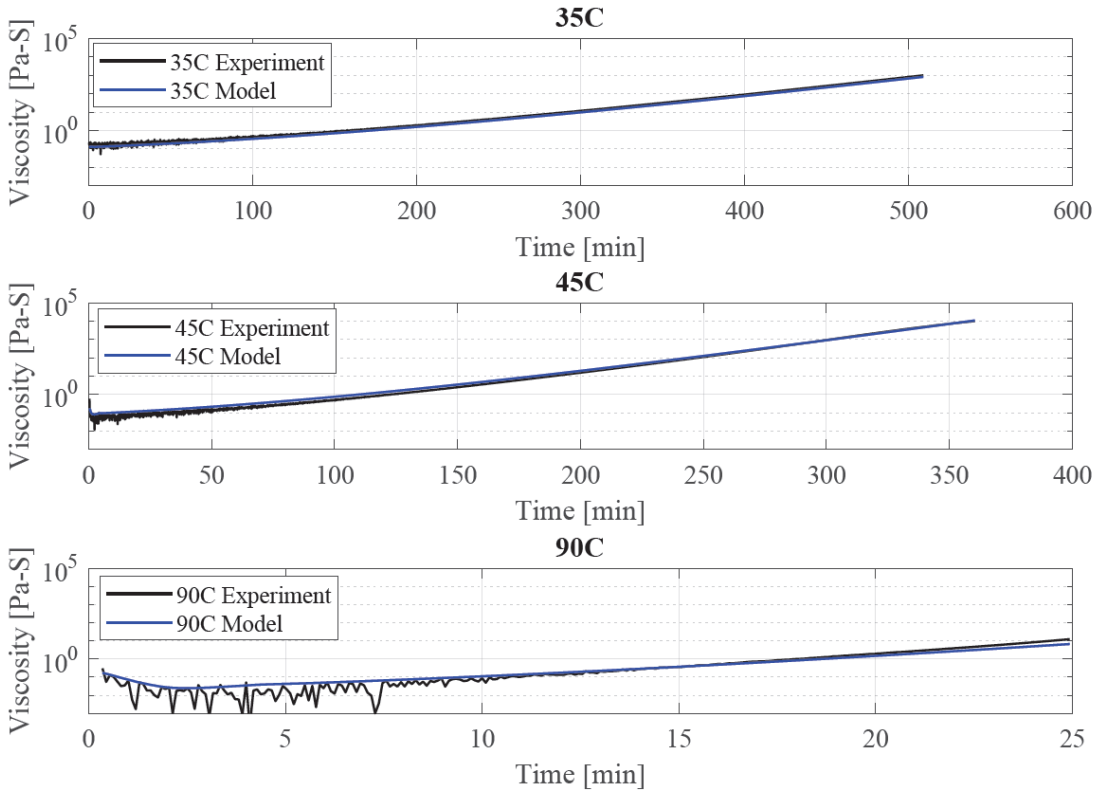

Figure 2: Experimental viscosity data versus fit Castro-Macosko model for Hexion EPIKOTE MGS RIMR 035c with an Epikure Curing Agent RIMH038

The Phase 2 values in Table 2 are noticeably different than what was presented in Phase 1 of this project. This is because the new Castro-Macosko model fit was done with 2 lower temperature data sets and 1 higher temperature data set, instead of all higher temperature data sets.

Table 2: Castro-Macosko model parameters that were fit with the isothermal rheometer runs

Parameter	Phase 2 Value	Phase 1 Value
$C\tau$	2.99e-8	2.7e-7
$T_g\ [K]$	4732.19	4.4e3
α_g	1.0	0.395
C_1	3.39	3.2
C_2	6.34	8.8

5 MODELING AND SIMULATION

A CAD representation of the 60-m spar cap was obtained and used to create a representative finite element model. The spar cap has a rectangular cross section along the majority of the length, but starts to taper around 55 m. During layup, a layer of flow media is placed along the entire length and width of the spar cap tool followed by the fiber glass stacking sequence. An omega tube, or feed line, is placed along one long edge of the fiber glass mat and connects to the flow media, while a vacuum line is located across the chord of the spar cap. This allows the vacuum to pull the resin from the omega tube and flow media through the fiberglass mat, wetting out the material. Figure 3 provides a cross sectional representation of the omega tube, vacuum line, composite, and flow media.

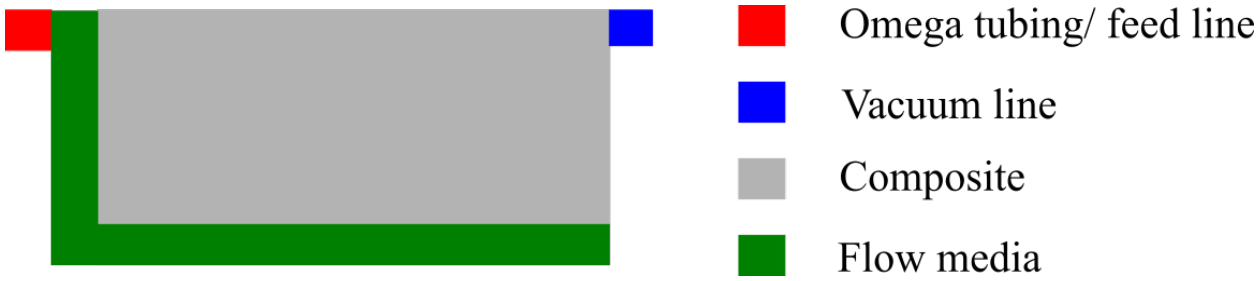

Figure 3: Cross section of the spar cap with omega tube, vacuum line, and flow media

A structured tet-mesh with linear elements was required for filling by the simulation software. The omega tube, composite stacking sequence, and flow media were all represented. A single layer of elements was used for the omega tubing and flow media, and the composite had 3 layers of elements modeled through the thickness. In reality, the omega tube has a circular cross section with an area of 506 mm^2. The FEM representation is square with a cross sectional area of 510 mm^2. The flow media was set to a 1 mm thickness. The final mesh had ~470,000 elements.

5.1 PAM-RTM Model

The filling simulation of the 60-m spar cap was completed using ESI software PAM-RTM. A heated filling simulation type was selected, and gravity was added. The initial degree of cure of the resin entering the system changes over time because the resin and hardener are mixed in a drum before being pulled into the fiberglass. If the epoxy in the drum exotherms a large amount, it can increase the curing rate. Experimental temperature measurements were made during the filling of one spar cap. The thermocouples were placed in the middle of the drum, along the wall of the drum, and in the ambient air to see if the epoxy exothermed during filling. Figure 4 shows that the drum center and wall kept relatively constant temperatures and only started to increase around 100 min into the filling. The ambient air stayed constant around 29 °C. Based on the experimental results, it was assumed that the drum temperature stayed constant at 30 °C for the filling simulation. The advancement in the degree of cure as resin entered the simulation was assumed to take the form of the cure results from the 35 °C experimental DSC test.

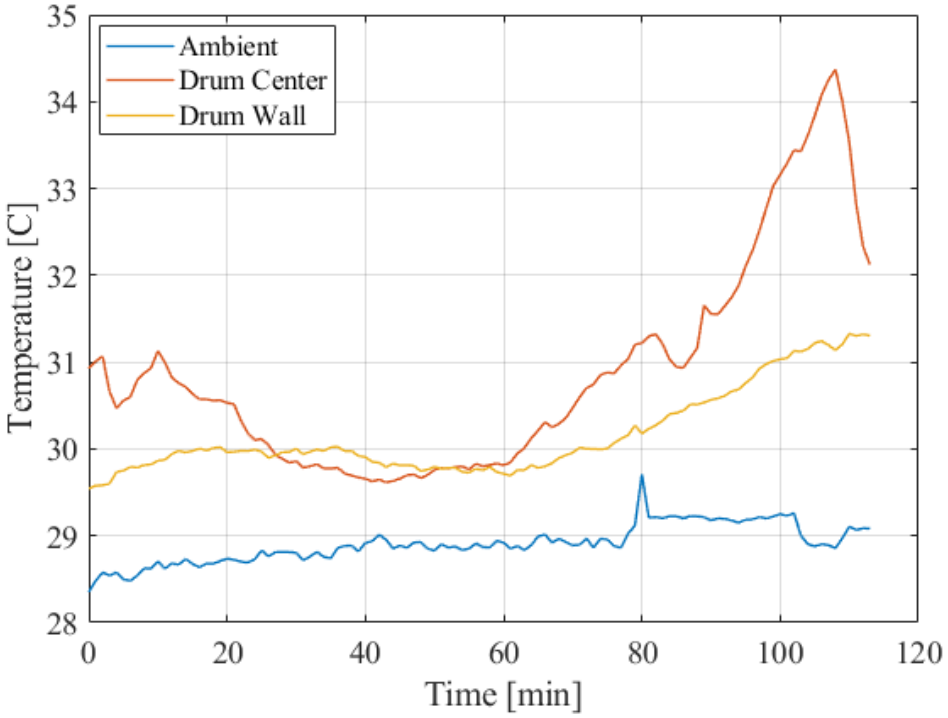

Figure 4: Experimental temperature measurements of the ambient air, drum center, and drum wall during filling of a 60-m spar cap

The viscosity settings and the cure kinetics for the resin were set to the parameters given in Table 1 and Table 2. The in-plane permeabilities for the fiberglass were set to 2.77e-10 m^2 and 4.37e-11 m^2 for k_1 and k_2 respectively. These values were based on experimental permeability tests from Phase 1. The through-thickness permeability of the fiberglass, k_3, was varied for the filling simulations to investigate the effect of k_3 on filling time. The permeabilities of the flow media were set to $k_1 = k_2 = k_3$= 5e-9 m^2. The permeability for the omega tube was estimated using an equivalent permeability equation provided by ESI Software for a geometry with a circular cross section.

$$K = \frac{a^2}{8} \tag{4}$$

In this case, a is the radius of the cross section. Using this equation, the omega tube permeability was defined as $k_1 = k_2 = k_3$ = 2.016e-5 m^2.

There were several temperature and processing conditions applied to the filling simulation. The bottom of the spar cap and flow media had a temperature boundary condition set to 35 °C because the mold was heated to that temperature throughout filling. The top surface of the spar cap and the omega tube had a convection boundary condition applied with the ambient air temperature set to 28.85 °C (seen experimentally in Figure 4). The convection coefficient was defined as 10 W/m^2-K. The vacuum line was not modeled with elements but instead applied as a process condition along the length of the spar cap opposite from the omega tube. The vent pressure was

set to 0 Pa. While the omega tube runs along the length of the spar cap, there is only one inlet location defined on the omega tube. The inlet pressure was set to 100 kPa, and the resin temperature was set to the average seen in the experimental drum measurements. The resin inlet was located near the halfway point down the longitudinal axis of the spar cap.

The filling simulation provides a temperature and DOC distribution during filling, as well as an estimated fill time and filling distribution. The filling time is compared to experiment, and the filling distribution is compared to qualitative observations during manufacturing. Experimental temperature data was obtained during the filling and curing process of a 60-m spar cap. The 14 distinct measurement locations were identified in the simulations and used for nodal temperature and DOC output comparisons. The filling simulation was run on a Dell OptiPlex 5040 with 6 Intel Core i7-6700 CPUs.

Four filling simulations were run to see the effect of the k_3 permeability on filling time. The permeability was varied from 1e-12 m^2 to 1e-14 m^2. Figure 5 shows that the filling time has an exponential relationship with the k_3 permeability for the 60-m spar cap. In addition, the lowest permeability of 1e-14 m^2 comes the closest to the experimental fill time (~120 min) with 103 min. These results indicate the k_3 parameter is crucial to simulating the filling of the spar cap. A reduced fill time will result in underestimated temperature and DOC distributions while an extended fill time would have the opposite problem. The filling simulation with permeability of 1e-14 m^2 was used for the remainder of the results presented.

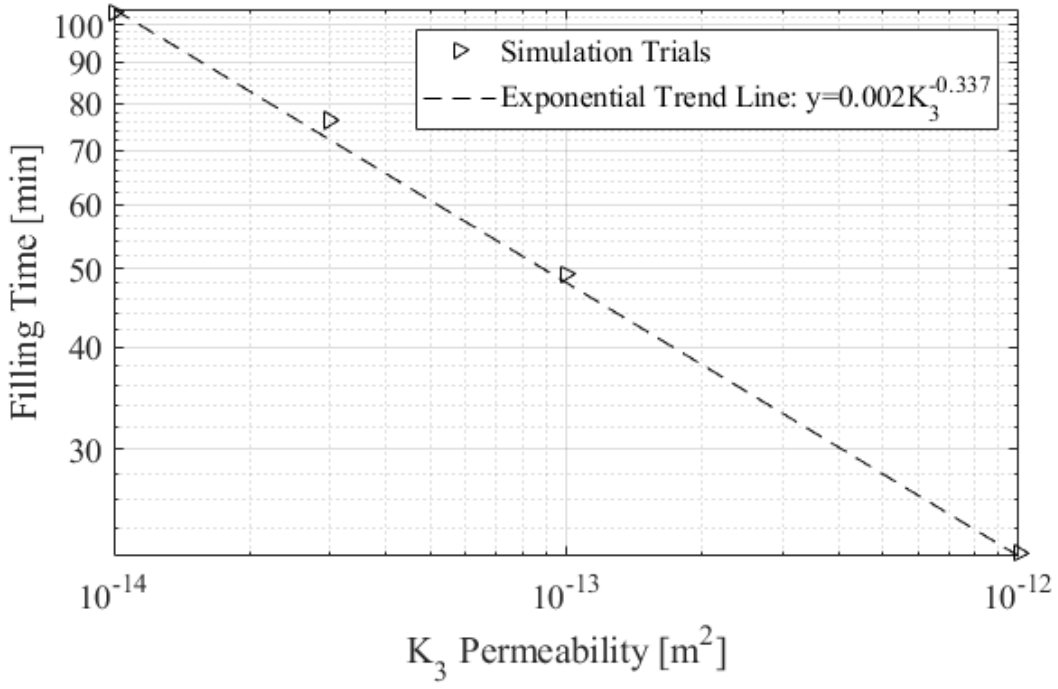

Figure 5: Filling time dependence on through-thickness permeability

A distribution map of the filling time (Figure 6) reveals how the flow front of the resin progressed through the spar cap. Upon initialization, the resin flowed swiftly down the omega tube and filled the thin ends of the spar cap first. The resin inlet was located about halfway down the longitudinal

axis of the spar cap, which also corresponds to the thickest section. The middle third of the spar cap, closest to the resin inlet, filled next. The edge with the vacuum line filled last.

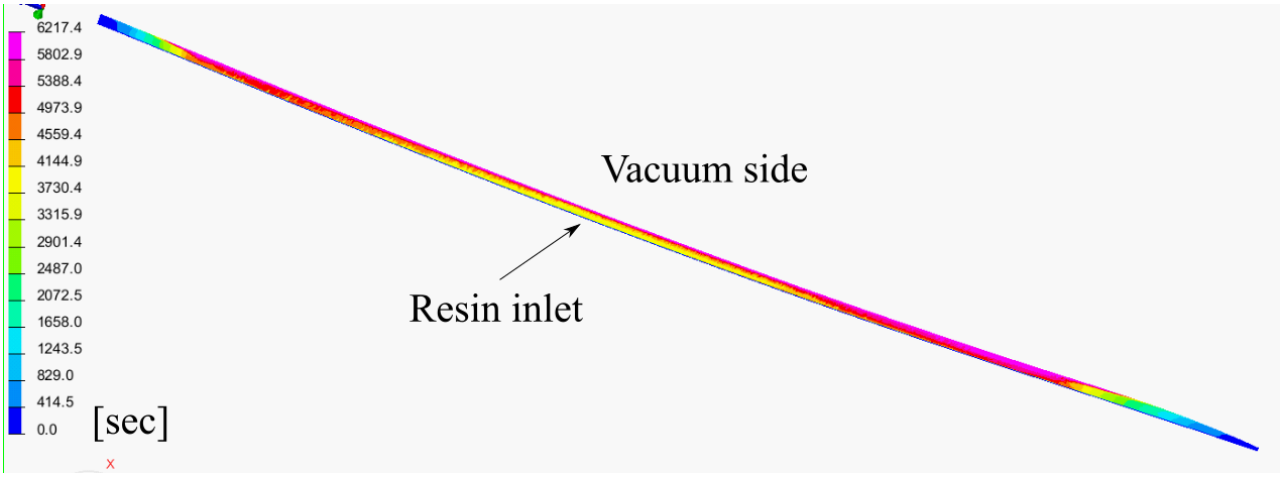

Figure 6: Top view of filling time distribution in seconds for the 60-m spar cap

The temperature and DOC development from the simulation was plotted at the 14 points that were measured experimentally. Each of these measurement points was located on the surface of the spar cap exposed to air. Therefore, the temperature measured during filling, should start off lower than the mold temperature of 35 °C. When comparing the filling simulation temperatures to the experimentally measured temperatures (Figure 7), there is a noticeable difference. While the initial temperatures for the simulation start at 28 °C, they quickly increase to a stable value of 35 °C. The source of this discrepancy was not identified in the duration of this project. However, additional material characterization, such as the glass fiber conduction value, may be a solution. Future work should investigate the cause of this and obtain a correction. During filling, the degree of cure increases relatively linearly with time. By the time filling is complete, parts of the spar cap are 20% cured. This again emphasizes the importance of capturing the correct filling time in order to predict the DOC properly.

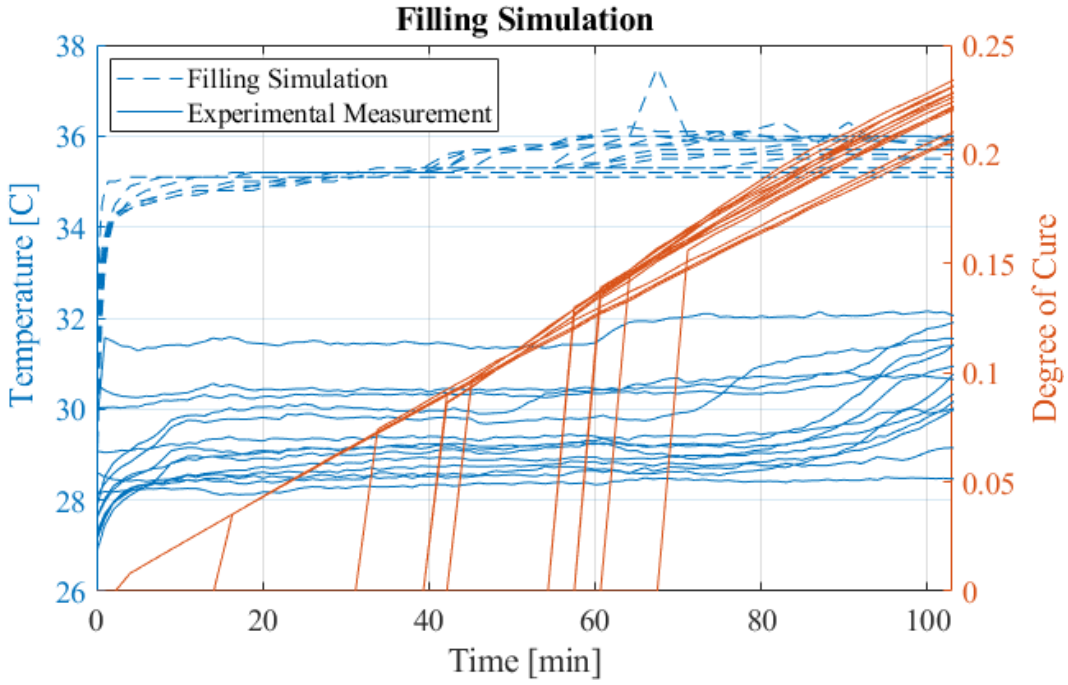

Figure 7: Filling simulation temperature and DOC development versus experimentally measured temperature

5.2 ABAQUS Model

Originally, the curing model was developed in ESI PAM-RTM software. However, once the software became unavailable, we implemented the curing work into an Abaqus model. The curing simulation was completed using a heat transfer analysis in Abaqus with a user-defined thermal material card, UMATHT. The temperature and DOC distributions from the filling simulation were extracted from the PAM-RTM results files (file extension: .erfh5) and collated to form initial condition distributions within Abaqus. A solid hex mesh with linear DC3D8 elements was implemented, and the flow media and omega tube elements were removed. The UMATHT subroutine implemented the autocatalytic model defined previously and updated the degree of cure and the rate of cure.

A time-dependent temperature boundary condition was applied to the bottom of the spar cap to recreate the curing profile the heated mold follows. Films were defined on the top and side surfaces of the spar cap to represent a heat sink from the ambient air. The convection coefficient for the films was defined using a correlation equation for a flat plate touching ambient air [6]. The heat transfer coefficient can be related to the geometry of the part

$$Nu_x = \frac{hx}{K_f} \tag{5}$$

Where h is the heat transfer coefficient, x is the characteristic length, Nu_x is the Nusselt number for the associated characteristic length, and K_f is the thermal conductivity of the fluid (in this case air).

The characteristic length for a flat plate is determined by the equation

$$x = \frac{A}{p} \tag{6}$$

Where A is the area of the plate and p is the perimeter. For the 60-m spar cap, the characteristic length is 0.27.

The Nusselt number is determined using the Rayleigh number associated with the characteristic length of the flat plate.

$$\begin{aligned} Nu_x &= 0.54\,(Ra_x)^{\frac{1}{4}} \text{ for } (10^4 \le Ra_x \le 10^7) \\ Nu_x &= 0.15(Ra_x)^{\frac{1}{3}} \text{ for } (10^7 \le Ra_x \le 10^{11}) \end{aligned} \tag{7}$$

The Rayleigh number is, in turn, calculated with the Prandtl number and the Grashof number. The Grashof number is dependent upon the characteristic length and is the ratio of buoyant forces to viscous forces in natural convection. The Prandtl number is the ratio of the momentum and thermal diffusivities [7] [8]. These are calculated with the following

$$Ra_x = Gr_x Pr = \frac{\left(g\beta\left(T_s - T_{\infty,f}\right)x^3\right)}{v\alpha} \tag{8}$$

Where g is gravity, $\beta = \frac{1}{T_{film}}$ where T_{film} is the average of the surface and ambient temperatures, T_s is the surface temperature, T_∞ is the ambient air temperature, v is the momentum diffusivity of the air, and α is the thermal diffusivity of the air. The ambient air properties for 25 °C were used with K_f= 26.24 mW/mK, α = 2.141e-5 m^2/s, and v = 1.562e-5 m^2/s.

In reality, the Rayleigh number changes as the spar cap exotherms. However, a constant Rayleigh number was assumed for simplification, and a surface temperature of $T_s = 35$ °C was used. This produced a Rayleigh number slightly greater than 10^7 meaning the bottom option for Equation (7) was implemented. This ultimately produced a heat transfer coefficient of 3.784 which was kept constant for all of the curing simulations.

Three different profiles were investigated with the curing simulations and can be seen in Figure 8. Profile 1 waits until after the part exotherms before it ramps up the mold temperature. This profile is known to produce quality parts, but it takes the longest time to complete. Profile 3 immediately ramps up temperature of the mold and is known to produce parts with thermal defects. Finally, Profile 2 uses an incremented heating approach and does not have associated results yet.

Each of the cure profiles starts after the filling simulation is completed. This allows the filling simulation to be constant between the three curing models. The primary outputs from the curing simulations include the temperature histories and distributions as well as the DOC histories and distributions. The curing simulations were run on a computing cluster using 4 nodes and a total of 80 CPUs.

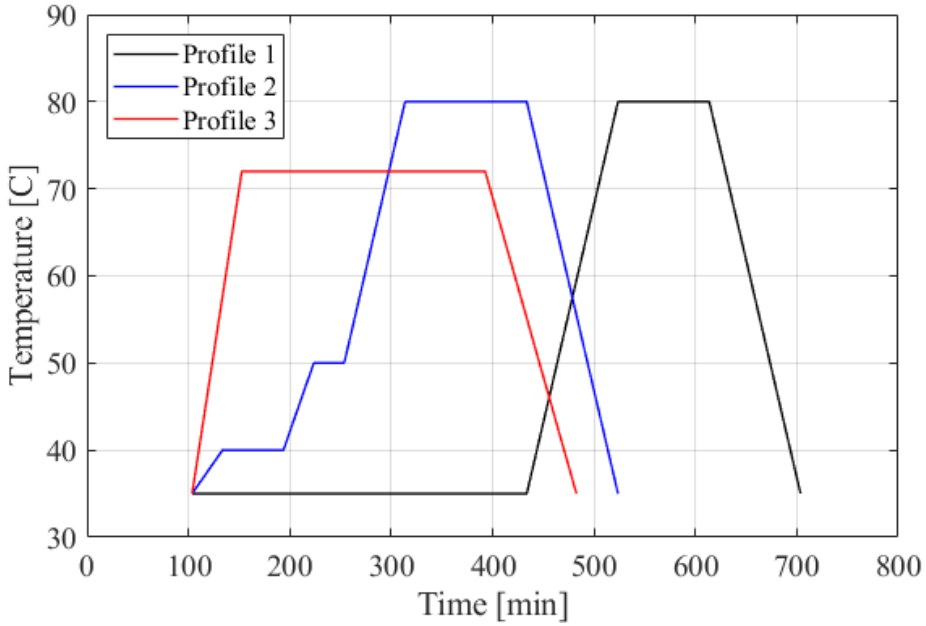

Figure 8: Temperature histories of the mold for 3 different curing profiles

Experimental temperature data was captured on a 60-m spar cap and subsequently compared to the cure simulation results for Profile 1. Figure 9 shows the increased temperature from the filling simulation carries over into the curing simulation. This is expected as the final results of the filling simulation were mapped onto the curing simulation. Immediately after filling, around 103 min in the simulation results, the spar cap begins to exotherm. The slope of the exotherm is steeper in the simulation than is seen in the experimental results. The peak exotherm results are slightly higher for the simulation versus the experiment as well, but they are within 5 °C. The mold heating of the simulation occurs before the experiment. The manufacturing method is not always precise in terms of timing, so it is likely that the mold heating after exotherm occurred at a later time than what was presented in the simulation. In addition, an increased conduction coefficient for the fiberglass can cause the temperature increase in the simulation to occur faster than the experiment. This was noted as a possibility for the near-instantaneous heating during the filling simulation as well. Once the mold is heated, there is a much steeper temperature increase in the experimental data versus the simulation, this is because insulation blankets are placed on the spar cap during manufacturing, and this was not captured in the simulation. Additional adjustments need to be made to the model to get the timing closer between the simulation and experiment, but the results show that the simulation method is producing similar results to the experiment.

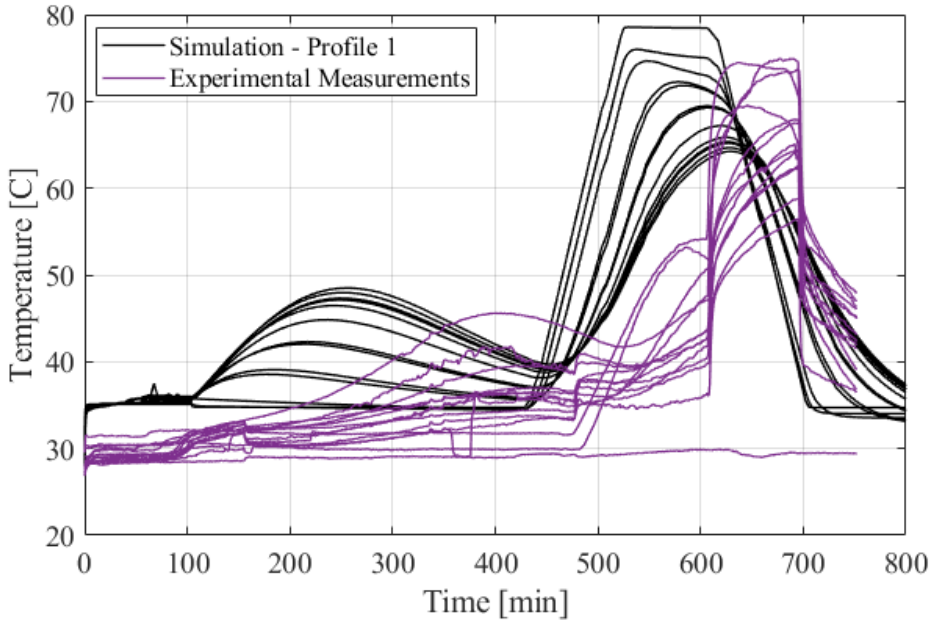

Figure 9: Temperature time history for simulated Profile 1 versus experimental measurements

When the temperature history of the three curing profiles are compared against one another, there are noticeable differences. Profile 3 has the highest temperature that is close to 20 °C larger than what is seen in Profile 1 or 2. Profile 3 is known to produce parts with defects, and the high temperature is a suspected cause. Profile 2 manages to be shorter than Profile 1, while still maintaining a similar temperature range. Profile 2 heats the mold before exotherm is complete, but it is still slower than Profile 3. This allows the exotherm to take place while the mold is heated but keeps the peak temperature at a similar value to Profile 1. These results indicate Profile 2 might be a valid option for a manufacturing cycle with a reduced curing time.

Figure 11 provides a comparison of the DOC versus time for each of the curing profiles. As expected, Profile 1 cures the slowest while Profile 3 cures the fastest. It is also interesting to note that Profile 1 has the largest spread in DOC data along the length of the spar cap. The ends of the spar cap have the slowest rate of cure and the rate increases going towards the center. Data was taken at 2.2 m, 6.5 m, 10.6 m, 14.7 m, 18.4 m, 23.2 m, 26.0 m, 30.3 m, 36.0 m, 40.3 m, 44.6 m, 48.9 m, 53.3 m, and 59.5 m along the span of the spar cap. This phenomenon is likely because the ends have less material and lower exothermic peaks than the center of the spar cap (see Figure 10).

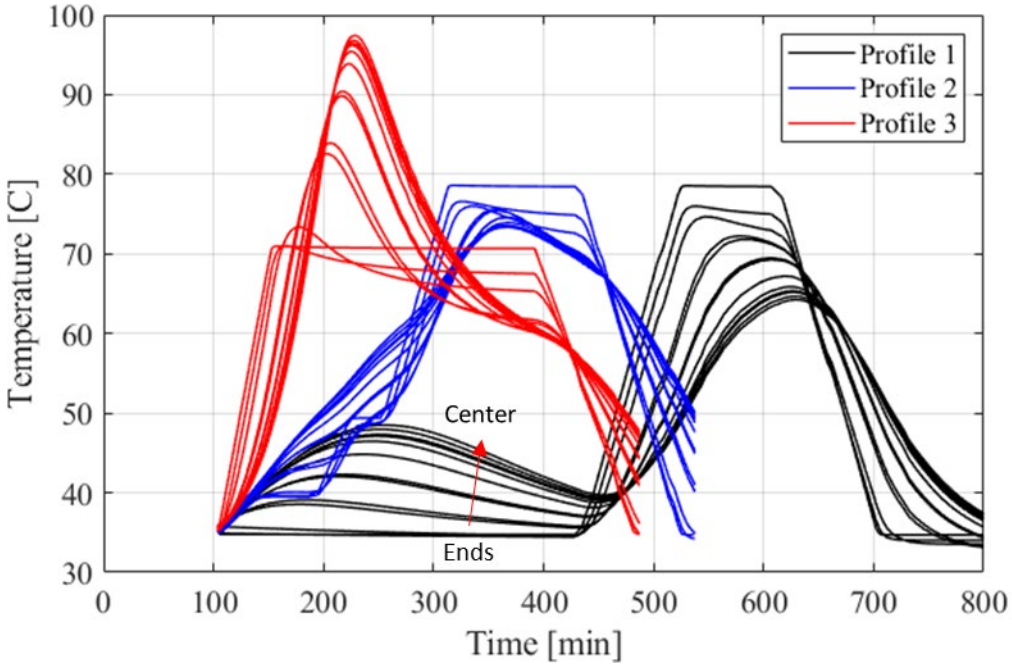

Figure 10: Temperature history comparison between 3 curing profiles

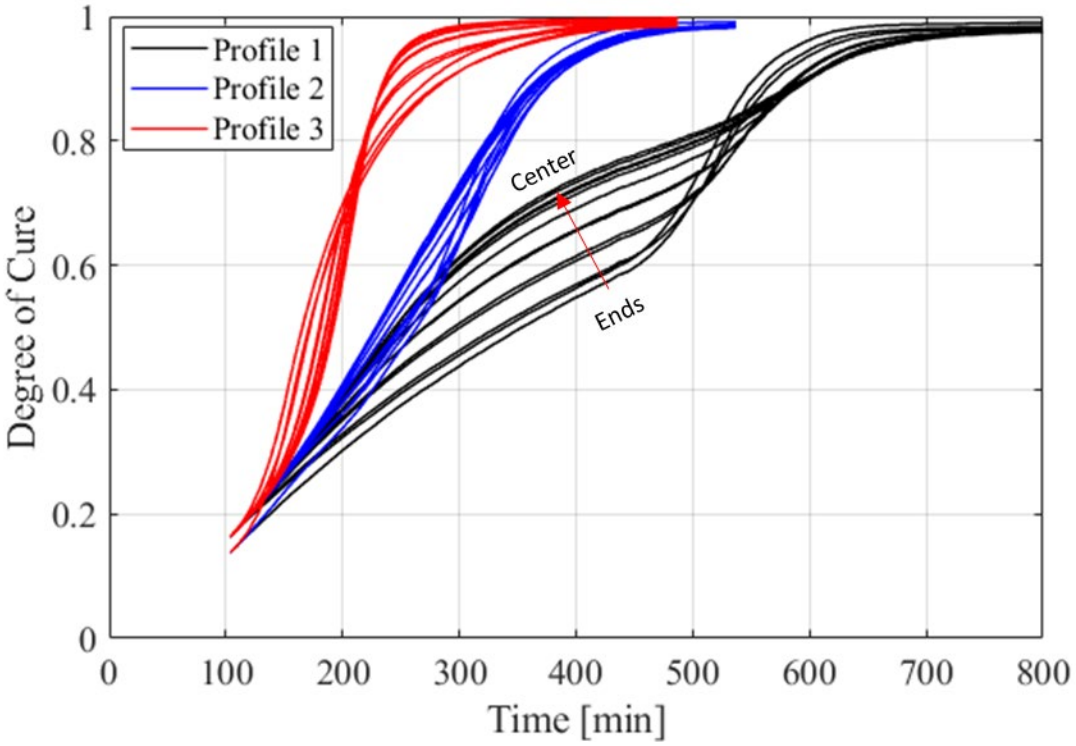

Figure 11: DOC history comparison between 3 curing profiles

5.3 Distortion Model

Prior to the end of the project, a distortion simulation was created using the ESI software PAM-DISTORT. The model mapped DOC distribution and temperature results from the curing simulation in PAM-RTM on to the distortion model. These distributions were in turn used to calculate the stress development associated with the resin system reaching gelation at different locations in the spar cap at different times. In addition, the interaction between the tool and the curing part via friction was to be modeled. However, access to the ESI software was removed before this could be accomplished.

Once the this occurred, we created the curing simulation in Abaqus with a user-defined material model. Unfortunately, there was not enough time left in the project to implement the distortion model in Abaqus as well. The plan was to model the friction between the tool and the spar cap as a function of DOC. As the part gels and hardens, the friction between the part and tool would increase. The stress build up from chemical shrinkage, gravity, and friction could be incorporated into the model to lead to the prediction of the thermal waves in the spar cap.

6 BENEFITS ASSESSMENT

This work demonstrates the possibilities available with manufacturing simulations. With further development, this simulation workflow could be used to optimize manufacturing cycles for wind turbine spar caps and other associated parts using the VARTM process. Simulations like these could save the company money in manufacturing cycle development and implementation.

7 COMMERCIALIZATION

The results from this work show that commercial finite element software can be used to capture the manufacturing process of real, in-production parts. With a finalized workflow, this work could be implemented in a company to optimize cycle times.

8 ACCOMPLISHMENTS

This project showed the merits of using simulations to assist in understanding of manufacturing processes and problems.

1. The cure kinetics and viscosity of the epoxy system were measured in lab and fit to an analytical model to be used in the process simulation
2. A filling simulation was created in PAM-RTM that was capable of capturing the filling time, DOC, and temperature distribution during the VARTM process.
3. A sensitivity study was completed on the through-thickness permeability parameter. The study showed that there is an exponential relationship between filling time and the permeability value.
4. A curing simulation was created in Abaqus that relied on a user-defined material model for the autocatalytic cure kinetics model. This simulation was capable of capturing the DOC distribution as a function of time as well as temperature distribution as a function of time.

9 CONCLUSIONS

This work presented a method for modeling the filling and curing of a 60-m wind turbine spar cap using characterized material properties. Model fits of the cure kinetics and resin viscosity

were incorporated into a PAM-RTM filling simulation that also captured necessary processing conditions associated with VARTM. The results of the filling simulation were used as initial conditions for a curing simulation which calculated the development of cure and the temperature history of the spar cap.

It was found that the filling time of the spar cap was exponentially dependent upon the through-thickness permeability of the fiberglass stacking sequence. Obtaining filling time results equivalent to experiment is vital to predicting the temperature and cure histories for a manufacturing cycle. However, this work showed that the proper material characterizations and model fits can produce filling times similar to that of experiment.

In addition, the curing simulation modeling an experimentally tested curing profile showed comparable temperature histories between the two. Slight differences can be explained by processing conditions not captured in the simulation such as insulation blankets, or imprecise timing in the mold temperature increases.

Comparing results from 3 curing profiles revealed that the degree of cure and the temperature of the spar cap are directly dependent upon timing of temperature increases in the mold as well as rate increases. Additional heating of the spar cap while the epoxy is exotherming can produce peak temperatures up to 20 °C above the highest mold temperature in the cycle.

Properly simulating the manufacturing process can allow for inexpensive experimentation with the cure cycle in order to reduce cycle time as much as possible and predict if a curing cycle will cause extensive defects.

10 RECOMMENDATIONS

Next steps for this work include adjusting the filling simulation to better match experimental temperature results and capturing the distortion and residual stresses associated with the curing process. Once the simulation workflow is completed, it is recommended to use the strategy of simulating manufacturing cycles to predict potential defects. Once trusted, the simulation method can be deployed for use within the wind turbine manufacturing industry.

11 REFERENCES

1. Sharp, Nathan, Cutting, Rebecca, and Sommer, Drew. *Thermal Instability in the Manufacturing of Wind Turbine Blade Spar Caps*. 2020. https://doi.org/10.2172/1633432. https://www.osti.gov/servlets/purl/1633432.
2. ESI Software, PAM-COMPOSITES 2020.5 PAM-FORM USER'S GUIDE, 2021.
3. Cutting, RA, Favaloro, AJ, Oquendo, E, Nolet S. *Multi-Physics Manufacturing Simulation of 60-Meter Wind Turbine Spar Cap.* Proceedings from CAMX 2021.
4. J. M. Kenny, *Determination of autocatalytic kinetic model parameters describing thermoset cure.* Journal of Applied Polymer Science, 51(4), 1994: 761-764. https://doi.org/10.1002/app.1994.070510424

5. J. M. Castro, C. W. Macosko, Studies of Mold Filling and Curing in the Reaction Injection Molding Process. AIChE Journal, 28(2), 1982: 250-260.
6. R. Goldstein, E. Sparrow, and D. Jones. *Natural convection mass transfer adjacent to horizontal plates*. International Journal of Heat and Mass Transfer, 16(5), 1973: 1025-1035.
7. E. Barocio. Fusion Bonding of Fiber Reinforced Semi-Crystalline Polymers in Extrusion Deposition Additive Manufacturing. Purdue University Graduate School.Thesis. 2020. https://doi.org/10.25394/PGS.7434068.v1
8. T. L. Bergman, F. P. Incropera, D. P. DeWitt and A. S. Lavine, Fundamentals of heat and mass transfer, John Wiley & Sons, 2011.